Energy Advances

ROYAL SOCIETY OF CHEMISTRY

PAPER

View Article Online
View Journal | View Issue

Cite this: *Energy Adv.*, 2023, 2, 1761

Long-stable solar energy capture and storage *via* negative thermal expansion regulated calcium-based particles†

Jingrui Liu, Yimin Xuan,* Liang Teng, Chen Sun, Qibin Zhu and Xianglei Liu

The 3rd concentrated solar power technology is considered a potential strategy to solve the energy shortage and achieve carbon neutrality in which the development of long-stable energy storage materials is the key to overcoming the intermittency and instability of solar power. Therefore, we present a calcium-based particle with a thermal expansion compensation strategy that enables high energy densities and long storage times. High measured energy densities of up to 1554 kJ kg^{-1}, long storage lifetimes of up to 260 cycles, and high spectral absorption of up to 90.8% are demonstrated in negative thermal expansion $NdMnO_3$/inert Al–Fe alkali metal element couples incorporated into calcium oxide structures. A set of evaluation indexes to quantitatively evaluate long-cycle heat storage performance is proposed. Based on the phenomenon that the thermal contraction of the $NdMnO_3$ lattice distortion counteracts the acidification volume expansion of calcium oxide, the thermal expansion compensation effect is proposed for the first time. This effect excellently ameliorates the problem of sintering and agglomeration and improves the recycling rate of calcium oxide from the perspective of microscopic thermal regulation. A new conceptual scheme is provided on long-storage-life solar thermochemical energy storage and continuous CO_2 capture technology.

Received 7th August 2023,
Accepted 20th September 2023

DOI: 10.1039/d3ya00379e

rsc.li/energy-advances

1. Introduction

The large-scale progression of industrialization urgently requires new renewable energy supplies. Among them, the clean energy pioneered by solar energy in the 3rd concentrated solar power technology has played an unprecedented role. As a sustainable and stable solar energy utilization technology, the solar-driven calcium-based thermochemical energy storage cycle has been extensively studied;[1,2] however, its sintering problem has led to its low utilization rate and poor economic benefit. Therefore, it is urgent to optimize and regulate it from the perspective of anti-sintering.

The calcium-based solar thermochemical cycle is divided into two processes as follows: calcium carbonate absorbs solar energy and decomposes to store energy, and calcium oxide carbonates to release heat and supply energy. During the heat release, due to the sintering of calcium oxide grains at high temperatures, a dense calcium carbonate product layer is formed on the surface, which prevents carbon dioxide from entering the interior of calcium oxide to react with it, and slows down the carbonation process.[3] At the same time, the reactivity decays rapidly with the increase in the number of cycles.[4] From the perspective of the change in free energy, if the free energy of the gas–solid interface is greater than that of the solid–solid interface, the solid atoms will transition from the solid–solid interface to the gas–solid interface, resulting in a decrease in the gas–solid contact area.[5] Macroscopically, the specific surface area is reduced, and the gas–solid reaction rate decreases.[6–8] Therefore, to inhibit sintering, relevant scholars have proposed that an inert carrier be added to calcium oxide grains to inhibit sintering and constrain the microscopic pore structure.[9–12] The principle is that the stability of the inert carrier is higher than that of calcium oxide. Ideally, it will stably adhere to the surface of calcium oxide, so the migration of calcium oxide grain boundaries will be affected by the pinning force of the inert carrier, thereby slowing down or inhibiting the grain sintering.[4] At present, the inert carriers with good effect mainly include MgO, $MgAl_2O_4$, ZnO, $Ca_{12}Al_{14}O_{33}$, SiO_2, Ca_2MnO_4, $CaZrO_3$, CuO, CoO, Y_2O_3, and $CaTiO_3$.[12–18] To improve the recycling efficiency of calcium-based materials, Kasper *et al.* added ZrO_2 (40%), and the CO_2 capacity was 35.5% after 50 cycles, but a lot of energy storage density was lost.[19] Teng *et al.* improved the spectral absorption by doping with multiple inert carriers (Fe–Mn), and the energy storage density

School of Energy and Power Engineering, Nanjing University of Aeronautics and Astronautics, Nanjing 210016, China. E-mail: ymxuan@nuaa.edu.cn; Fax: +86-25-84890688; Tel: +86-25-84890688

† Electronic supplementary information (ESI) available. See DOI: https://doi.org/10.1039/d3ya00379e

was 1057 kJ kg^{-1} after 15 cycles.[20] Sun *et al.* also used binary inert carrier doping to modify dolomite, making its spectral absorption rate reach 73.22% and energy density 770 kJ kg^{-1} after 30 cycles.[21] Our previous work also screened and proved these inert carriers. It is believed that doping with Fe element can form black compounds with calcium oxide at high temperatures, which can improve the spectral absorption rate of the particles due to the extremely poor light absorption ability of pure calcium carbonate.[22] At the same time, the doping of Al elements can effectively improve the cycle stability by inhibiting the migration of calcium oxide grains.[23] Therefore, on this basis, we are exploring new channels of anti-sintering from a new perspective.

Although plenty of research efforts have been devoted to improving the cyclic stability and energy density of calcium-based materials through doping with inert carriers, the anti-sintering effect of inert carriers is mainly to inhibit the migration of crystal grains. The migration of crystal grains is related to the surface free energy, particle size, volume fraction of the inert carrier, and the interaction force between the inert carrier and calcium oxide, so simply adding an inert carrier to regulate the sintering effect is far from enough.[24,25] At the same time, the inert carrier can separate the calcium oxide grains, which hinders the agglomeration but cannot counteract the growth and expansion caused by the reaction. During the carbonation process, the growth of calcium oxide will break through the bound interface, resulting in agglomeration and sintering. Therefore, from the perspective of counteracting the growth expansion, this work introduces a negative thermal expansion precursor (NTEP), through its negative thermal expansion (NTE) in the exothermic temperature range of calcium oxide, to offset the growth expansion caused by the carbonation reaction and inhibit the grain, which plays a role in regulating the sintering of calcium oxide. NTE is caused by anomalous mechanisms such as phase transitions, shortened bond lengths, rigid unit modes, electronic effects, and magnetostriction. Natural materials such as perovskites have NTEs, but their applications are limited due to their narrow NTE temperature range, large thermal anisotropy, and low degree of design freedom;[26] therefore, relevant scholars began to develop new NTE materials. Martinek and Hummel[27] reported the negative thermal expansion of ZrW_2O_8, and subsequently, Sleight and Mary *et al.*[28] demonstrated its isotropic NTE over a wide temperature range. At present, there are many kinds of NTE materials, and the common ones mainly include various framework oxides, zeolites, cyanides, anti-perovskite nitrides and metal–organic frameworks.[29–31] A typical one is ZrW_2O_8; however, despite its good NTE properties, it is metastable below 777 °C and decomposes into ZrO_2 and WO_3 in the temperature range of 777 to 1105 °C, which is not suitable for carbonation.[32]

Herein, we propose a new strategy for achieving the regulation of the cycling stability and anti-sintering of calcium oxide particles by introducing NTE $NdMnO_3$. The coefficient of thermal expansion (CTE) of the composite calcium-based material is targeted and supervised, effectively alleviating the thermally induced cracking caused by the CTE mismatch of different doped materials. At the same time, the spectral absorption, and the stable and durable energy storage performance of the material have been improved by leaps and bounds, which provide a new scheme for industrial long-cycle-durable solar thermochemical energy storage and CO_2 capture.

2. Results

2.1 Composition and performance

Porous micron-sized composite calcium-based materials (CM) were synthesized by the sol–gel method as outlined in the SI. The molar ratios of Fe, Al and Nd elements in doped ferric nitrate (Aladdin 99%), aluminum nitrate (Aladdin 99%), and $NdMnO_3$ were 5 : 10 : 5, 5 : 10 : 10, and 5 : 10 : 20. For the convenience of description, the samples mentioned below are uniformly numbered: 5 : 10 : 5, 5 : 10 : 10, and 5 : 10 : 20. The XRD spectrum in Fig. 1(a) shows that the main component of the composite calcium-based material is calcium oxide, and the basic main diffraction peaks can be well indexed. In the range of 27–30°, the main diffraction peaks of all doped calcium oxide samples were slightly shifted. This is because a certain amount of dopant cations (Fe, Al) enters the calcium oxide lattice during the solid-state synthesis process, resulting in lattice distortion, which causes the shift of the diffraction peak. For composite calcium-based particles, new oxides are formed after multi-element doping: $Ca_2(Al, Fe^{3+})_2O_5$, $NdCaAl_3O_7$, $CaAl_2O_4$ and other components. At the same time, after doping NTEP, it still appeared in the form of $NdMnO_3$, indicating that most of the Nd did not react with Ca to form composite oxides. This provides direct evidence for the subsequent regulation of negative thermal expansion properties.

During the carbonation of calcium oxide, CO_2 is adsorbed on the surface of calcium oxide to form calcium carbonate, which causes volume expansion and thus the internal pores are blocked. However, the doping of NTEP can customize high CO_2 adsorption CM with near-zero thermal expansion properties. In particular, the three-dimensional porous structure in the composite is combined with isotropic negative thermal expansion. The NTEP is used as a thermal expansion compensator, which greatly slows down the effect of reducing the yield of adsorbed CO_2 due to volume expansion and blocking the channel to achieve the behavior role of control of calcium oxide in the carbonation reaction.[33] Fig. 1(b) shows the linear thermal expansion curves of the calcium-based material before and after doping with NTEP. Between 500 °C and 800 °C, the thermal expansion coefficient of $NdMnO_3$ decreased with the increase in temperature, which showed good negative thermal expansion performance with an average negative thermal expansion coefficient of -5.29×10^{-4} K^{-1}. When the temperature reached 800 °C, the negative thermal expansion coefficient of $NdMnO_3$ reached -1.68×10^{-3} K^{-1}, and this negative thermal expansion performance is currently the best. However, the linear thermal expansion coefficient of the calcium-based material without NTEP increased gradually with the increase in temperature, and the thermal expansion coefficient at 800 °C

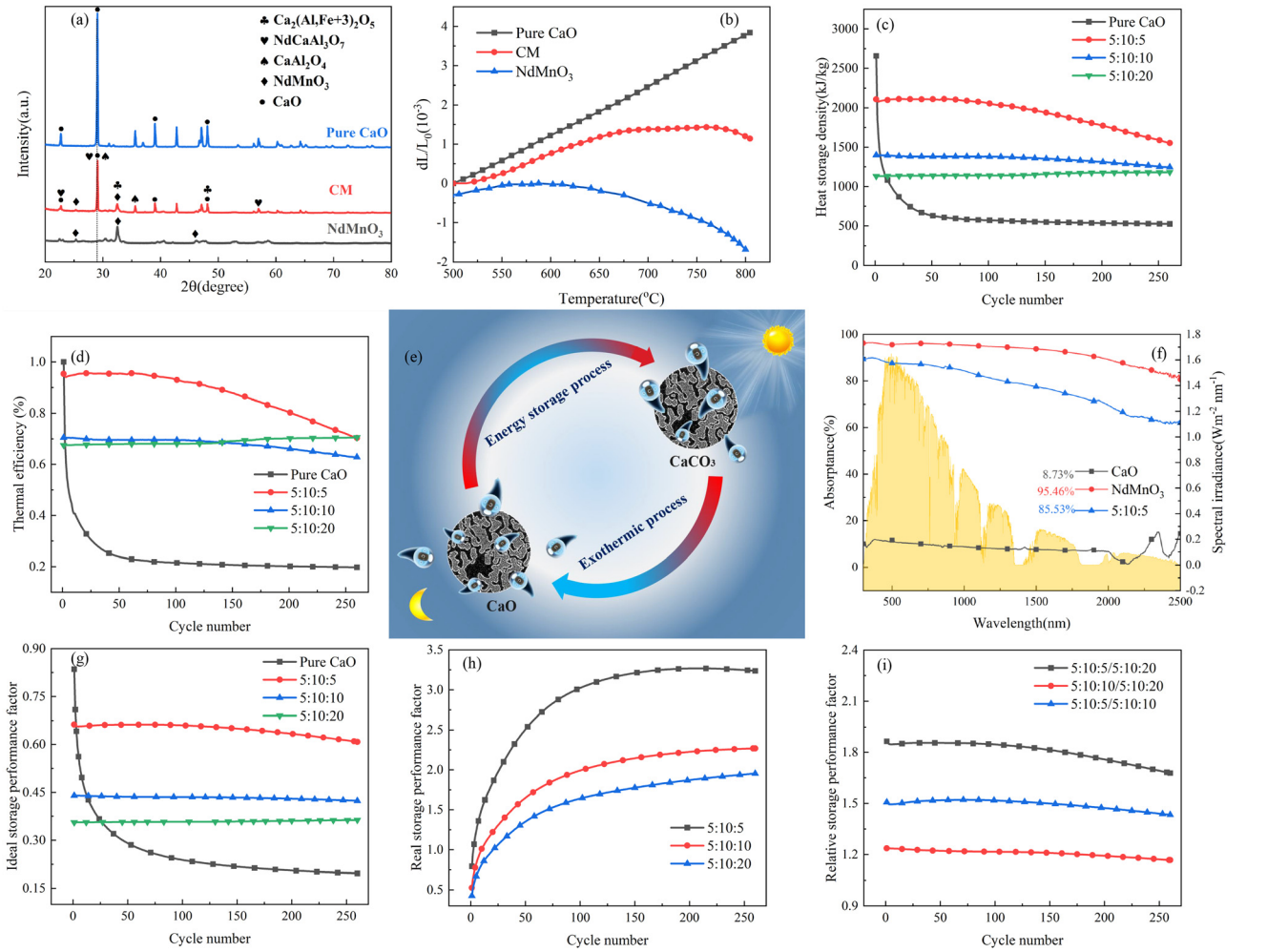

Fig. 1 Composition and performance parameters: (a) the phase composition of the three materials, (b) the linear thermal expansion coefficient at different temperatures; (c) and (d) the heat storage density and thermal efficiency, (e) the schematic diagram of Ca-looping, and (f) the spectral absorption. (e), (h) and (i) The ideal, real and relative storage performance factors, respectively.

was 3.84×10^{-3} K^{-1}. When the temperature increased from 500 °C to 695 °C, the thermal expansion coefficient of the calcium-based material after adding $NdMnO_3$ increased from -1.11×10^{-6} K^{-1} to 1.38×10^{-3} K^{-1}, and then when the temperature reached 695 °C, a turning point of the thermal expansion coefficient occurred. From 695 °C to 800 °C, the negative thermal expansion coefficient of CM decreased from 1.38×10^{-3} K^{-1} to 1.14×10^{-3} K^{-1}. The thermal expansion coefficient of the CM decreased by 70.3% at 800 °C as compared with pure calcium oxide. The results show that doping NTEP has an ideal thermal matching effect and can regulate the positive thermal expansion of calcium oxide, which is an effective strategy for alleviating sintering.

Multiple cycles of energy storage and release will lead to the sintering and agglomeration of particles to reduce energy storage density. Therefore, NTEP was doped to ensure the reutilization rate of calcium-based particles to reduce energy consumption and cost. Fig. 1(c) demonstrates the energy storage density of particles with different doping ratios for 260 cycles. Here, the following thermochemical energy storage density and efficiency are defined to evaluate the cycle and heat storage performances of calcium-based materials with negative thermal expansion effects:

$$E_n = \frac{m_{CaCO_3,n} - m_{CaO,n}}{m_{i,n}} \cdot \Delta H / M_{CO_2} \quad (1)$$

$$\eta_n = \frac{E_n}{E_{i,n}} = \frac{(m_{CaCO_3,n} - m_{CaO,n})\Delta H / M_{CO_2}}{(m_{i,n} - m_{CaO,n})\Delta H / M_{CO_2}} = \frac{m_{CaCO_3,n} - m_{CaO,n}}{m_{i,n} - m_{CaO,n}} \quad (2)$$

where $m_{CaCO_3,n}$ and $m_{CaO,n}$ indicate the mass of particles at the end of the calcination/carbonation process of cycle n; $m_{i,n}$ represents the original mass of calcium oxide particles, M_{CO_2} is the molar mass of CO_2, ΔH is the molar reaction enthalpy. After 260 cycles, the heat storage density of pure calcium oxide changed from 2655 kJ kg^{-1} to 525 kJ kg^{-1}, and the thermal efficiency dropped by 80.23%. After 260 long cycles, the heat storage density of particles decreased by the 5 : 10 : 10 doping

ratio changed from 2107 kJ kg^{-1} to 1554 kJ kg^{-1} and only decreased by 26.25%, which not only showed good cycle stability but also maintained a high energy storage density.

However, the above parameters are all defined for single-cycle energy storage, and none of them can evaluate the heat storage performance of the composite over a long span. Therefore, for multi-cycle heat storage, we proposed a new set of concepts, namely, the ideal storage performance factor (P_{ideal}), real storage performance factor (P_{real}), and relative storage performance factor ($P_{relative}$), respectively. These parameters are respectively defined as follows:

$$P_{ideal} = \frac{\sum_{i=1}^{n} \Delta E_{drop}(i)}{\Delta E_{ideal}.n} \quad (3)$$

$$P_{real} = \frac{\sum_{i=1}^{n} \Delta E_{drop}(i)}{\sum_{j=1}^{n} \Delta E_{drop}(j)} \quad (4)$$

$$P_{relative} = \frac{\sum_{i=1}^{n} \Delta E_{drop1}(i)}{\sum_{j=1}^{n} \Delta E_{drop2}(i)} \quad (5)$$

where $\Delta E_{drop}(i)$ is the energy storage density of the doped particles in the ith cycle, ΔE_{ideal} and ΔE_{pure} are the ideal and real energy storage densities of pure calcium-based particles, and n is the number of cycles.

The storage performance factor for 260 long cycles has been calculated in Fig. 1(g), (h), and (i). After 260 cycles, the ideal storage performance factor of particles with a doping ratio of 5 : 10 : 5 decreased from 0.663 to 0.608, with an attenuation of 8.3%, while the attenuation ratio of pure calcium oxide particles was 71.5%. For the real energy storage factor, the calcium-based particles with a mixing ratio of 5 : 10 : 5 were 3.24 times that of pure calcium oxide after 260 cycles. This shows that the calcium-based particles regulated by negative thermal expansion can greatly alleviate the attenuation of the heat storage performance caused by sintering and agglomeration, and provide a reliable long-term stable energy storage and CO_2 capture approach for subsequent industrial applications. To further highlight the long-term heat storage performance of calcium-based particles with different dosing ratios, the relative energy storage capacity is given in Fig. 1(i) for the relative energy storage factor. The relative energy storage factors of the three blended particles are stable for up to 260 cycles. Among them, the 5 : 10 : 5 sample is always about 1.8 times that of 5 : 10 : 20, the 5 : 10 : 10 sample is 1.5 times that of 5 : 10 : 20, and the 5 : 10 : 5 sample is 1.2 times that of 5 : 10 : 10. This shows that the particles with a doping ratio of 5 : 10 : 5 can provide a higher energy storage density under the premise of maintaining a relatively stable energy storage capacity.

As the key to solar energy storage, in addition to high energy storage density, composite calcium-based particles (CM) also need excellent spectral absorption ability to be directly driven by solar energy. Due to pure calcium oxide being white, and it is still white when converted into calcium carbonate, the spectral absorption effect is extremely poor, which cannot meet the requirements of directly capturing and converting solar energy. Therefore, it is necessary to physically modify and dope metal elements to form black composite oxides or carbonates to improve the spectral absorption performance of the material. The reflectance of the material was measured by a UV IR spectrometer (Carry 5000, Agilent Technologies) multiple integrating spheres, and the average spectral absorptivity at 300–2500 nm was obtained according to the weighted integral formula of the absorptivity and standard solar irradiance. Fig. 1(d) shows that the spectral absorption rate of sol–gel CM with doping of 5 : 10 : 5 reached 85.53%, which is 9.8 times higher than that of pure calcium oxide. It showed excellent spectral absorption performance and provides a good base material for the direct utilization of solar energy.

$$A = \frac{\int_{300\ nm}^{2500\ nm} \alpha(\lambda) I_{AM1.5}(\lambda) d\lambda}{\int_{300\ nm}^{2500\ nm} I_{AM1.5}(\lambda) d\lambda} \quad (6)$$

$\alpha(\lambda)$, $I_{AM1.5}$ and λ are the spectral absorptivity, standard solar irradiance, and wavelength of each band, respectively.

2.2 Microscopic mechanism

In the process of multiple cycles of CO_2 adsorption, the adsorption performance gradually decreases with the increase in the number of cycles, which is mainly due to the sintering of calcium oxide grains. In general, sintering occurs at temperatures well below the melting point of solid materials. The Tammann temperature of $CaCO_3$ is 533 °C, and the carbonation temperature (700 °C) used in this work is higher than the Tammann temperature of $CaCO_3$ (533 °C). Therefore, the material will first reach the Tammann temperature before the reaction, at which time the diffusion of ions and cavities will be activated, and grain boundary fusion will occur, forming crystal/grain agglomeration.[5,9] The agglomeration of grains reduces the specific surface area of the particles, resulting in a decrease in porosity and activity, which slows down the carbonation rate and the degree of the solid adsorption reaction in the next cycle. The schematic diagram of the sintering mechanism of calcium oxide particles before and after doping NTEP is shown in Fig. 2.

The structural optimization and electronic properties of $NdMnO_3$ were calculated based on the density functional theory (DFT); the phonon spectrum was obtained by the finite displacement method, and then the thermal expansion coefficient of the material decreasing from 600 to 800 °C was calculated by the quasi-harmonic approximation (QHA) in Fig. S2 (ESI†). The cell structure of calcium oxide particles is face-centered cubic. During the carbonation of calcium oxide, external CO_2 molecules diffuse through porous structures between grains and electron transfer occurs at high temperatures. A deep chemisorption potential well was found, and then CO_2 transitioned from a high potential energy state to a low potential energy state, forming covalent bonds with calcium oxide molecules and generating $CaCO_3$ by a chemisorption

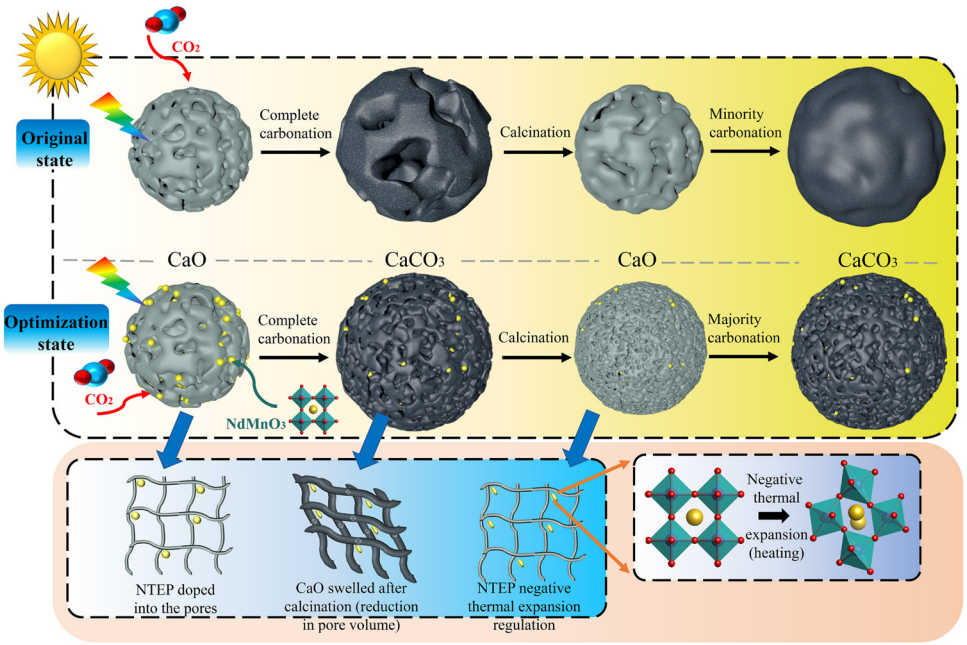

Fig. 2 Schematic diagram of the sintering mechanism of calcium oxide particles before and after doping with NTEP.

reaction.[9,34] However, the $NdMnO_3$ at room temperature is an orthorhombic perovskite structure, with Mn atoms as the body center, O atoms as the face center, and Nd atoms as the octahedron vertex. When the temperature rises to 600 °C, the molecular phase begins to change, and the MnO_6 octahedron begins to distort, transforming from the orthorhombic phase to the cubic phase, the bond length becomes shorter, the structure is distorted, and the lattice volume becomes smaller. This expands the space available for the calcium oxide lattice to absorb CO_2 molecules, resulting in more opportunities for calcium oxide to participate in the reaction. Fig. 3 is a scanning electron micrograph of particles doped with NTEP. Because the intensity of the backscattered electron signal is related to the average atomic number of the pattern, the higher the average

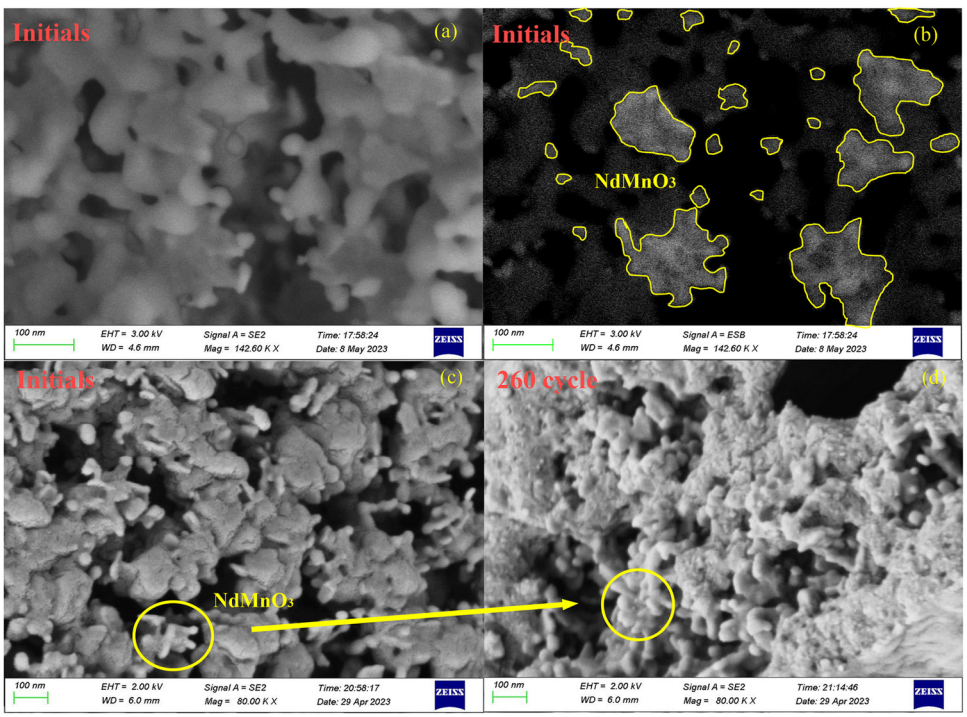

Fig. 3 Microscopic SEM images of calcium oxide particles doped with NTEP.

atomic number, the stronger the backscattered electron signal and the higher the brightness. The average atomic number of $NdMnO_3$ is much larger than that of calcium oxide, so the bright spot in Fig. 3(b) is $NdMnO_3$. At the same time, it can be seen from the comparison of Fig. 3(c) and (d) that after 260 cycles, $NdMnO_3$ partially migrates and agglomerates and the negative thermal expansion effect area of $NdMnO_3$ becomes smaller, resulting in sintering at the position where there is no $NdMnO_3$-filled calcium oxide. The introduction of $NdMnO_3$ with the NTE effect reduces the residual stress of calcium oxide to generate calcium carbonate, thereby slowing down the tendency of the established structure to be destroyed by thermal stress. Macroscopically, the volume expansion is alleviated, and the sintering problem of particles is effectively solved through the thermal expansion regulation effect.

2.3 Application promotion

To make them suitable for the large-scale industrialization reaction, the particles will be broken and worn down during the continuous tumbling and collision process. However, micron-sized particles do not have mechanical strength due to their small size, agglomeration, and coagulation, which lead

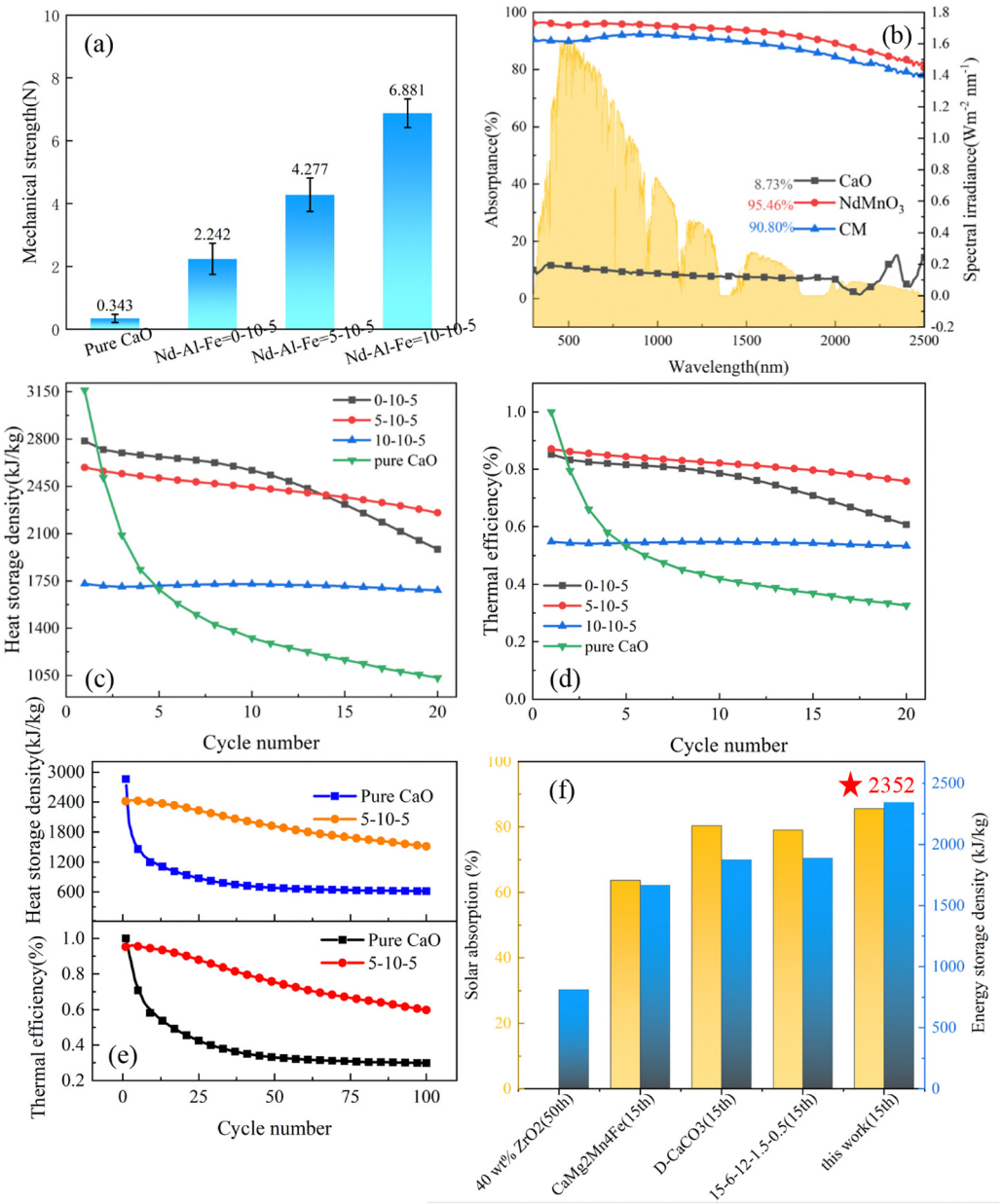

Fig. 4 Comprehensive properties of millimeter-scale particles: (a) the average mechanical strength of the particles under different doping, (b) the spectral absorption, (c) and (d) the heat storage density and thermal efficiency of particles with different doping ratios under 20 cycles, (e) the heat storage density and thermal efficiency of particles with Nd : Al : Fe = 5 : 10 : 5 and pure calcium oxide under 100 cycles, and (f) the comparison of energy storage density and solar absorption in different references and this work.

to an extremely poor fluidization effect. In addition, the separation of powder is difficult, which is not conducive to transportation and storage, and the leakage will affect health after being inhaled by the human body. Therefore, composite particles with a diameter of 1 mm are synthesized to ensure mechanical strength during fluidization. A manual pressure testing machine (Lingyue, LYYS-100N) was adopted to measure the mechanical strength of calcium oxide particles in different proportions. According to the method of taking the average value of ten measurements, the mechanical strength parameters of the particles were accurately obtained. Fig. 4(a) shows that the average mechanical strength of pure calcium oxide particles was 0.343 N, which is very easy to break, while the average mechanical strength of the sample doped with a molar ratio of Nd : Al : Fe = 5 : 10 : 5 was 4.277 N. The measurement errors were also calculated, and the errors of the four groups of particles after ten measurements were 0.132, 0.498, 0.534 and 0.455, respectively. The results show that with the increase in doping, the average mechanical strength of the particles gradually increased. After doping with $NdMnO_3$, the mechanical strength was maintained above 2 N, which can maintain a certain mechanical strength during the fluidized collision process and is suitable for multi-cycle thermochemical energy storage systems. The spectral absorptivity of the particles was also thoroughly tested. Fig. 4(b) shows that the spectral absorptivity of the CM particles of 5–10–5 was 10.4 times higher than that of pure calcium oxide particles, and 6.16% higher than that of micron-sized particles, reaching 90.8%, which can realize extremely efficient light-to-heat conversion performance.

As shown in Fig. 4(c), the proportion of doped NTEP increased and the initial energy storage density gradually decreased. The initial energy storage density of particles with a doping ratio of Nd : Al : Fe =5 : 10 : 5 (2589 kJ kg^{-1}) was lower than the initial energy storage density (3162 kJ kg^{-1}) of pure calcium oxide but after 20 cycles, the energy storage density of doped particles remained at 2253 kJ kg^{-1}, which is much higher than that of pure calcium oxide particles (1034 kJ kg^{-1}). Meanwhile, the thermal efficiency of particles with different doping ratios under 20 cycles was tested. The results show that the thermal efficiency at the beginning of the cycle decreased with the increase of the dopant content, while the cycle stability increased with the increase of the dopant content. To balance thermal efficiency, energy storage density and cycle stability, among the three groups of different doping components, the composite calcium oxide particles with Nd : Al : Fe = 5 : 10 : 5 showed the best comprehensive performance. Therefore, the 5–10–5 sample was further tested in a long-cycle experiment. Fig. 4(e) shows that the initial energy storage density of pure calcium oxide was 2863 kJ kg^{-1} but only 616 kJ kg^{-1} remained after 100 cycles. However, although 5–10–5 also had a downward trend, the energy storage density was 1516 kJ kg^{-1} after 100 cycles and the thermal efficiency was 59.8%. Compared with pure calcium oxide particles, the heat storage performance increased by 146.2%. This indicates excellent anti-sintering and heat storage properties.

To intuitively demonstrate the advantages of the negative thermal expansion strategy proposed in this work, the results of energy storage density and spectral absorptivity of different calcium-based particles in the references are compared at the same time. Fig. 4(f) shows that the solar absorption rate of 5–10–5 particles treated with the thermal expansion compensation effect was 90.8%, and the maximum energy storage density after 15 cycles was 2352 kJ kg^{-1}, both of which are significantly higher as compared with previous work, which shows its great potential for solar thermochemical energy storage. The specific data are shown in Table S1 (ESI†).

Fig. 5(a) displays the morphological changes of pure calcium oxide particles before and after 100 cycles on two scales. Before

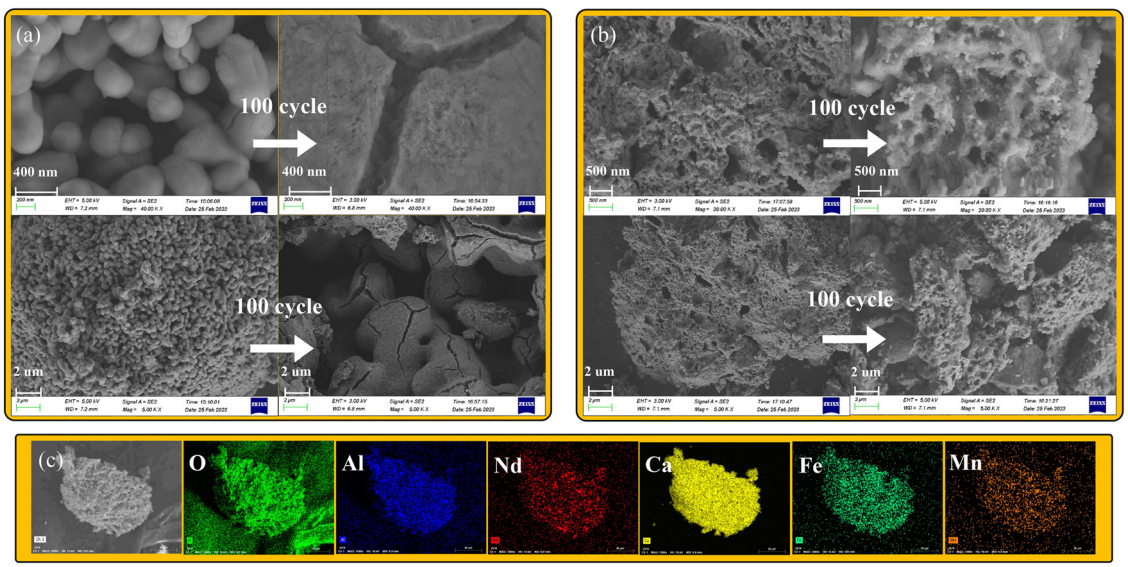

Fig. 5 Morphology changes and element distribution: (a) and (b) the evolutions of pure calcium oxide and composite calcium-based particle morphology (SEM); (c) the energy spectrum distribution of composite materials.

carbonation, the size of the calcium oxide grains was about 300 nm, and the arrangement was close. However, after 100 cycles, the grain boundaries of calcium oxide disappeared and the phenomenon of aggregation occurred. This indicates that in the process of high-temperature carbonation, calcium oxide cells absorb carbon dioxide and convert it to calcium carbonate, expanding in volume, causing solids to move closer together and form large polymers covering the reaction surface. With the increase in the number of cycles, the grain size of calcium oxide gradually increased, resulting in a more serious agglomeration process and lower porosity. Besides, the morphology of calcium oxide grains doped with $NdMnO_3$ and Al–Fe oxides did not change significantly after 100 cycles in Fig. 5(b), and nanopores and micropores were present, indicating that the doped materials effectively regulated the agglomeration process between calcium oxide grains. The energy spectrogram in Fig. 5(c) shows that the doped elements are relatively uniformly distributed, indicating that the physical synthesis method can achieve uniform doping effects.

3. Conclusion

This work proposes a calcium cycle anti-sintering control strategy that uses the negative thermal expansion properties of $NdMnO_3$ to slow down the sintering and agglomeration of calcium oxide particles. By adjusting the coefficient of thermal expansion (CTE) of the composite calcium-based material, the thermally induced cracking caused by the mismatch of the CTE of different doped materials can be effectively alleviated. A set of evaluation indexes to quantitatively evaluate long-cycle heat storage performance is proposed, where after 260 cycles of material-modified calcium oxide particles, the energy storage density of particles doped by 5 : 10 : 5 remains at 1554 kJ kg^{-1}. The spectral absorptivity increased by 980%, and the mechanical strength of the particles increased to 4.277 N. The stable and durable energy storage performance of the material has been improved by leaps and bounds. The morphology changes before and after 260 cycles were observed from the microscopic scale; $NdMnO_3$, with the NTE effect, reduced the residual stress of calcium carbonate generated from calcium oxide through lattice distortion, thereby slowing down the tendency of the established structure to be destroyed by thermal stress. From the perspective of atomic vibration, the phonon spectrum of $NdMnO_3$ was obtained by the finite displacement method, and the thermal expansion coefficient of the material was calculated by QHA, which further verified its negative thermal expansion characteristics. Macroscopically, the volume expansion was alleviated, and the sintering problem of particles was effectively solved through the thermal expansion regulation effect. This provides a new strategy for thermochemical energy storage materials for large-scale industrial applications.

Data availability

Synthesis methods, measurements and computational methods can be found in the ESI.† Upon request to the corresponding author, further information supporting this study can be made available.

Author contributions

Jingrui Liu: conceptualization, methodology, experiment, writing – original draft preparation, visualization. Yimin Xuan: conceptualization, methodology, supervision, resources, project administration, eriting – review & editing, funding acquisition. Liang Teng: provision of study materials, investigation. Chen Sun: implementation of the computer code and supporting algorithms. Qibin Zhu: data curation, formal analysis, experimental assistance. Xianglei Liu: writing – review & editing, project administration.

Conflicts of interest

There are no conflicts to declare.

Acknowledgements

This work is supported by Basic Science Center Program for Ordered Energy Conversion of the National Natural Science Foundation of China (no. 51888103) and the Key International Cooperation Projects of the National Natural Science Foundation of China (grant no. 51820105010).

References

1 R. Chacartegui, A. Alovisio, C. Ortiz, J. M. Valverde, V. Verda and J. A. Becerra, *Appl. Energy*, 2016, **173**, 589–605.
2 Y. Xu, T. Zhang, B. Lu, C. Luo, F. Wu, X. Li and L. Zhang, *Energy Convers. Manage.*, 2021, **250**, 114886.
3 J. Liu, Y. Xuan, L. Teng, Q. Zhu and X. Liu, *Chem. Eng. Sci.*, 2022, **248**, 117212.
4 J. S. Dennis and R. Pacciani, *Chem. Eng. Sci.*, 2009, **64**, 2147–2157.
5 X. K. Tian, S. C. Lin, J. Yan and C. Y. Zhao, *Chem. Eng. J.*, 2022, **428**, 131229.
6 W. Ostwald, *Z. Phys. Chem.*, 1897, **22U**, 289–330.
7 R. L. Coble, *J. Am. Ceram. Soc.*, 1973, **56**, 461–466.
8 F. F. Lange and B. J. Kellett, *J. Am. Ceram. Soc.*, 1989, **72**, 735–741.
9 Y. Hu, H. Lu, W. Liu, Y. Yang and H. Li, *Chem. Eng. J.*, 2020, **396**, 125253.
10 Z. Li, Y. Liu and N. Cai, *Chem. Eng. Sci.*, 2013, **89**, 235–243.
11 Y. Hu, W. Liu, H. Chen, Z. Zhou, W. Wang, J. Sun, X. Yang, X. Li and M. Xu, *Fuel*, 2016, **181**, 199–206.
12 J. Sun, S. Bai, K. Li, Y. Zhou, Y. Chen, L. Liu and Z. Zhou, *ACS Appl. Energy Mater.*, 2022, **5**, 4903–4915.
13 K. T. Møller, A. Berger, M. Paskevicius and C. E. Buckley, *J. Alloys Compd.*, 2022, **891**, 161954.
14 M. Lanchi, A. Spadoni, S. Sau, A. C. Tizzoni, F. Varsano, N. Corsaro, L. Turchetti, R. Liberatore, A. D. G. D. Mauro, T. Delise, E. Mansi, M. A. Murmura and M. C. Annesini,

presented in part at the SOLARPACES 2020:26th International Conference on Concentrating Solar Power and Chemical Energy Systems, 2022.
15 C. Gao, Y. Zhang, D. Li and M. Li, *ACS Omega*, 2022, **7**, 45443–45454.
16 Y. Zhou, Z. Zhou, L. Liu, X. She, R. Xu, J. Sun and M. Xu, *Energy Fuels*, 2021, **35**, 18778–18788.
17 H. Li, Y. Chen, L. Leng and Y. Hu, *Energy Fuels*, 2021, **35**, 12610–12618.
18 Z. Ge, F. Jiang, Q. Chen, L. Wang, Y. Ding and H. Chen, *Chem. Eng. J.*, 2022, **444**, 136353.
19 K. T. Møller, A. Ibrahim, C. E. Buckley and M. Paskevicius, *J. Mater. Chem. A*, 2020, **8**, 9646–9653.
20 L. Teng, Y. M. Xuan, X. L. Liu and Y. L. Ding, *AIChE J.*, 2022, **68**, 17546.
21 S. B. Bai, J. Sun, L. Liu, Y. Da, Z. J. Zhou, R. L. Wang, Y. F. Guo and C. W. Zhao, *Sol. Energy Mater. Sol. Cells*, 2022, **239**, 111659.
22 Y. Da, Y. Xuan, L. Teng, K. Zhang, X. Liu and Y. Ding, *Chem. Eng. J.*, 2020, **382**, 122815.
23 C. Song, X. Liu, Y. Xuan, H. Zheng, K. Gao, L. Teng, Y. Da, C. Li, Y. Li and Y. Ding, *Sci. China: Technol. Sci.*, 2021, **64**, 2142–2152.
24 V. Manovic, E. J. Anthony, G. Grasa and J. C. Abanades, *Energy Fuels*, 2008, **22**, 3258–3264.
25 A. Balamurugan, G. Balossier, S. Kannan, J. Michel, A. H. Rebelo and J. M. Ferreira, *Acta Biomater.*, 2007, **3**, 255–262.
26 L. Wu, B. Li and J. Zhou, *ACS Appl. Mater. Interfaces*, 2016, **8**, 17721–17727.
27 C. A. Martinek and F. A. Hummel, *J. Am. Ceram. Soc.*, 1970, **53**, 159–161.
28 T. A. Mary, J. S. O. Evans, T. Vogt and A. W. Sleight, *Science*, 1996, **272**, 90–92.
29 C. R. Morelock, B. K. Greve, L. C. Gallington, K. W. Chapman and A. P. Wilkinson, *J. Appl. Phys.*, 2013, **114**, 213501.
30 L.-M. Zhao, Y.-G. Cheng, H.-S. Hao, J. Wang, S.-H. Liu and B.-S. Zhang, *Chin. Phys. B*, 2018, **27**, 096501.
31 W. Miller, C. W. Smith, D. S. Mackenzie and K. E. Evans, *J. Mater. Sci.*, 2009, **44**, 5441–5451.
32 C. Yang, J. Li, D. Yang, S. Li, Y. Qin, S. Meng and S. Du, *ACS Sustainable Chem. Eng.*, 2019, **7**, 14747–14755.
33 R. O. Fleming, S. Goncalves, A. Davarpanah, I. Radulov, L. Pfeuffer, B. Beckmann, K. Skokov, Y. Ren, T. Li, J. Evans, J. Amaral, R. Almeida, A. Lopes, G. Oliveira, J. P. Araujo, A. Apolinario and J. H. Belo, *ACS Appl. Mater. Interfaces*, 2022, **14**, 43498–43507.
34 C. T. Rettner, D. J. Auerbach, J. C. Tully and A. W. Kleyn, *J. Phys. Chem.*, 1996, **100**, 13021–13033.